Science
AAAS

Supplementary Materials for

TARGETED DOWN REGULATION OF CORE MITOCHONDRIAL GENES DURING SARS-COV-2 INFECTION

Joseph W. Guarnieri[1,2], Joseph M. Dybas[1,2], Hossein Fazelinia[1,2], Man S. Kim[1-3], Justin Frere[4], Yuanchao Zhang[1,2], Yentli Soto Albrecht[1,2], Deborah G. Murdock[1], Alessia Angelin,[1] Larry N. Singh[1,2], Scott L. Weiss[1], Sonja M. Best[2,5], Marie T. Lott[1], Henry Cope[6], Viktorija Zaksas[2,7], Amanda Saravia-Butler[2,8,9], Cem Meydan[2,10], Jonathan Foox[10], Christopher Mozsary[10], Yared H. Kidane[2,11], Waldemar Priebe[2,12], Mark R. Emmett[2,13], Robert Meller[2,14], Urminder Singh[2,15], Yaron Bram[10], Benjamin R. tenOever[4], Mark T. Heise[16], Nathaniel J. Moorman[16], Emily A. Madden[16], Sharon A. Taft-Benz[16], Elizabeth J. Anderson[16], Wes A. Sanders[16], Rebekah J. Dickmander[16], Victoria K. Baxter[16], Stephen B. Baylin[2,17], Eve Syrkin Wurtele[2,15], Pedro M. Moraes-Vieira[2,18], Deanne Taylor[1,2], Christopher E. Mason[2,10,19], Jonathan C. Schisler[2,16], Robert E. Schwartz[2,10], Afshin Beheshti[2,20,21]†*, Douglas C. Wallace[1,2,22]†*

*Corresponding authors: WallaceD1@chop.edu and afshin.beheshti@nasa.gov

This PDF file includes:

Materials and Methods

EXPERIMENTAL MODEL AND SUBJECT DETAILS

Human nasopharyngeal swab sample collection for RNA-seq analysis

Patient specimens were processed as described in Butler et al.(*1*). Briefly, nasopharyngeal swabs were collected using the BD Universal Viral Transport Media system (Becton, Dickinson and Company, Franklin Lakes, NJ) from symptomatic patients. Total Nucleic Acid (TNA) was extracted using automated nucleic acid extraction on the QIAsymphony and the DSP Virus/Pathogen Mini Kit (Qiagen).

Human autopsy tissue collection for RNA-seq analysis (5-8 controls & 35-36 patients)

The full methods of the patient sample collection from the autopsy patients are currently available in the Park et al. (*2*). All autopsies are performed with the consent of the next of kin and permission for retention and research use of tissue. Autopsies were performed in a negative pressure room with protective equipment including N-95 masks; brain and bone were not obtained for safety reasons. All fresh tissues were procured prior to fixation and directly into Trizol for downstream RNA extraction. Tissues were collected from lung, liver, lymph nodes, kidney, and heart as consent permitted. For GeoMx, RNAscope, trichrome and histology tissue sections were fixed in 10% neutral buffered formalin for 48 hours before processing and sectioning. These cases had a post-mortem interval of less than 48 hours. For bulk RNA-seq tissues, post-mortem intervals ranged from less than 24 hours to 72 hours (with 2 exceptions - one at 4 and one at 7 days - but passing RNA quality metrics) with an average of 2.5 days. All deceased patient remains were refrigerated at 4ºC prior to autopsy performance. Host profiling was done on 39 patients that died from COVID-19 and healthy controls from organ donor remnant tissues (n = 3).

Virus lines

SARS-CoV-2 Washington strain (isolate USA-WA1/2020, NR-52281) were provided by the Center for Disease Control and Prevention and obtained through BEI Resources, NIAID, NIH. Cell lines Vero E6 (African green monkey [Chlorocebus aethiops] kidney, CVCL_0574; female) were obtained from ATCC (https://www.atcc.org/). Cells were cultured in Dulbecco's Modified Eagle Medium (DMEM) supplemented with 10% FBS and 100 U/mL penicillin and 100mg/mL streptomycin. Cells were tested for the presence mycoplasma bi-weekly using MycoAlert Mycoplasma Detection Kit (lonza), They were not authenticated by an external service but were derived directly from ATCC.

SARS-CoV-2 propagation and infections

SARS-CoV-2 was propagated in Vero E6 cells in DMEM supplemented with 2% FBS, 4.5 g/L D-glucose, 4 mM L-glutamine, 10 mM Non-Essential Amino Acids, 1 mM Sodium Pyruvate and 10 mM HEPES using a passage-2 stock of virus. Three days after infection supernatant containing propagated virus was filtered through an Amicon Ultra 15 (100 kDa) centrifugal filter (Millipore Sigma) at 4000 rpm for 20 minutes. Flow through was discarded and virus was resuspended in DMEM supplemented as described above. Infectious titers of SARS-CoV-2 were determined by plaque assay in Vero E6 cells in Minimum Essential Media supplemented with2% FBS, 4 mM L-glutamine, 0.2% BSA, 10 mM HEPES and 0.12% NaHCO3 and 0.7% agar. All work involving

live SARS-CoV-2 was performed in the CDC/USDA-approved BSL-3 facility with institutional biosafety requirements.

SARS-CoV-2 hamster model

Three-5-week-old male Golden Syrian hamsters (Mesocricetus auratus) were obtained from Charles River. Hamsters were acclimated to the CDC/USDA-approved BSL-3 facility for 2-4 days before viral infection. The hamsters were housed in a temperature-controlled room (20-22ºC), on a 12 h light/dark cycle (08:00 – 20:00 lights on), with food (PicoLab Rodent Diet 20 5053) and water provided ad libitum. All hamsters were in good health and demonstrated normal behavior until the infection. All animal experiment procedures, breeding and ethical use were performed in accordance with the guidelines set by the Institutional Animal Care and Use Committee. Hamsters were anesthetized by intraperitoneal injection with a ketamine HCl/xylazine solution (4:1) before being intranasally inoculated with 100 pfu of SARS-CoV-2 isolate USA-WA1/2020 in PBS (or PBS only as a control) in a total volume of 100 ml. All animal experiments were performed on at least two separate occasions. Blinded treatment groups used mice throughout the study limited investigator subjectivity.

SARS-CoV-2MA10- murine model

All experiments were conducted using approved standard operating procedures and safety conditions for SARS-CoV-2 in BSL3 facilities designed following the safety requirements outlined in the Biosafety in Microbiological and Biomedical Laboratories, 6th edition, the United States Department of Health and Human Services, the Public Health Service, the Centers for Disease Control and Prevention (CDC), and the National Institutes of Health (NIH). All experiments and researchers followed protocols approved by the Institutional Animal Care and Use Committee (IACUC) at The University of North Carolina (UNC), Chapel Hill, NC.

The mice were housed in the UNC ABSL3 facility on a 12:12 light cycle using autoclaved cages (Tecniplast, EM500), irradiated Bed-o-Cob (ScottPharma, Bed-o-Cob 4RB), ad libitum irradiated chow (LabDiet, PicoLab Select Rodent 50 IF/6F 5V5R), and autoclaved water bottles. Animals used in this study included female 16-week-old C57BL/6J (B6) (The Jackson Laboratory stock 000664) or 10-12-week-old BALB/cAnNHsd (BALB/c) (Envigo order code 047) mice, purchased directly from vendors.

Mice were infected following light sedation, using 50 mg/kg ketamine and 15 mg/kg xylazine, by intranasal inoculation with 10^4 pfu SARS-CoV-2-MA10 (3) diluted in 50 µL PBS or PBS alone (mock infection). Blinded treatment groups used mice throughout the study limited investigator subjectivity. Mice were euthanized by an overdose of isoflurane anesthetic and lung tissues collected for subsequent processing.

METHOD DETAILS

RNA-seq of nasopharyngeal swab COVID-19 patient samples

RNA isolation and library preparation are fully described in Butler, et al. (1). Briefly, library preparation on all the nasopharyngeal swab samples' total nucleic acid (TNA) were treated with DNAse 1 (Zymo Research, Catalog # E1010). Post-DNAse digested samples were then put into the NEBNext rRNA depletion v2 (Human/Mouse/Rat), Ultra II Directional RNA (10 ng), and Unique Dual Index Primer Pairs were used following the vendor protocols from New England Biolabs. Kits were supplied from a single manufacturer lot. Completed libraries were quantified

3

by Qubit or equivalent and run on a Bioanalyzer or equivalent for size determination. Libraries were pooled and sent to the WCM Genomics Core or HudsonAlpha for final quantification by Qubit fluorometer (ThermoFisher Scientific), TapeStation 2200 (Agilent), and qRT-PCR using the Kapa Biosystems Illumina library quantification kit.

RNA-seq of COVID-19 autopsy tissue samples

RNA isolation and library preparation is detailed in Park, et al.(*2*). Briefly, autopsy tissues were collected from lung, liver, lymph nodes, kidney, and heart and were placed directly into Trizol, homogenized and then snap frozen in liquid nitrogen. At least after 24 hours these tissue samples were then processed via standard protocols to isolate RNA. New York Genome Center RNA sequencing libraries were prepared using the KAPA Hyper Library Preparation Kit + RiboErase, HMR (Roche) in accordance with manufacturer's recommendations. Briefly, 50-200ng of Total RNA was used for ribosomal depletion and fragmentation. Depleted RNA underwent first and second-strand cDNA synthesis followed by adenylation, and ligation of unique dual indexed adapters. Libraries were amplified using 12 cycles of PCR and cleaned-up by magnetic bead purification. Final libraries were quantified using fluorescent-based assays including PicoGreen (Life Technologies) or Qubit Fluorometer (Invitrogen) and Fragment Analyzer (Advanced Analytics) and sequenced on a NovaSeq 6000 sequencer (v1 chemistry) with 2x150bp targeting 60M reads per sample.

RNA-seq of COVID-19 hamster tissue samples

RNA from hamster tissues was extracted using TRIzol Reagent (ThermoFisher Scientific), followed by overnight precipitation at -20 °C, and quantified using a NanoDrop (ThermoFisher Scientific). 1 mg of total RNA was enriched for polyadenylated RNA species and prepared for short-read next-generation sequencing using the TruSeq Stranded mRNA Library Prep Kit (Illumina) according to the manufacturer's instructions. Sequencing libraries were sequenced on an Illumina NextSeq 500 platform. Fastq files were generated using bcl2fastq (Illumina) and aligned to the Syrian golden hamster genome (MesAur 1.0, ensembl) using the RNA-seq Alignment application (Basespace, Illumina). Golden Hamster ensembl genes were matched to homologous external gene names, human homolog ensembl genes, and human associated homo-log gene names using BioMart (*4, 5*). OrthoFinder was used to generate orthologous human ensembl gene ids and gene names (*6*). After further filtering and quality control, R package edgeR (*7*) was used to calculate RPKM and Log2counts per million (CPM) matrices as well as perform differential expression analysis.

RNA-seq of COVID-19 murine tissue samples

RNA from inferior mouse lung lobes was extracted using TRIzol Reagent (ThermoFisher Scientific), followed by overnight precipitation at -20 °C, and quantified using a NanoDrop (ThermoFisher Scientific). Ribosomal RNA from 1000 ng total extracted RNA was depleted using a NEBNext rRNA Depletion Kit (Human/Mouse/Rat) (New England Biolabs Inc.). The remaining RNA was used to produce the sequencing libraries using the NEBNext Ultra II Directional RNA Library Prep Kit for Illumina (New England Biolabs Inc.) with AMPure XP (Beckman Coulter Life Sciences) for all bead cleanup steps. The libraries were sequenced on a NovaSeq 6000 System, using a NovaSeq 6000 SP Reagent Kit v1.5 (Illumina).

QUANTIFICATION AND STATISTICAL ANALYSIS

Analysis of nasopharyngeal swab RNA-seq data

The nasopharyngeal swab samples were analyzed comparing COVID-19 viral infection to the negative patients as previously described in Butler et al. (*1*)and the DESeq2 (*8*)was utilized to generate the differential expression data. Using all clinical samples there were a total of N = 216 COVID+ samples and 519 COVID negative samples. There also included 17 positive (Vero E6 cells) and 33 negative (buffer) controls.

Analysis of autopsy RNA-seq data

The full methods for the analysis of autopsy patients can be found in the Park et al. (*2*). Briefly, RNA-seq data was processed through the nf-core/rnaseq pipeline (*9*). This workflow involved adapter trimming using Trim Galore! (https://github.com/FelixKrueger/TrimGalore), read alignment with STAR (*10*), gene quantification with Salmon (*11*), duplicate read marking with Picard MarkDuplicates (https://github.com/broadinstitute/picard), and transcript quantification with StringTie (*12*). Other quality control measures included RSeQC, Qualimap, and dupRadar. Alignment was performed using the GRCh38 build native to nf-core and annotation was performed using Gencode Human Release 33 (GRCH38.p13). FeatureCounts reads were normalized using variance-stabilizing transform (vst) in DESeq2 package in R for visualization purposes in log-scale (*8*). Differential expression of genes was calculated by DESeq2. Differential expression comparisons were performed as either COVID+ cases versus COVID- controls for each tissue specifically, correcting for sequencing batches with a covariate where applicable, or pairwise comparison of viral levels from the lung as determined by Counter data.

Metabolic modeling and downstream statistical analyses

We simulated the optimal fluxes of each metabolic reaction for each RNA-seq sample, using an adjusted version of a context specific constraint based metabolic modeling method (*13, 14*). We constructed a context specific genome scale metabolic model for each RNA-seq sample, by subsetting metabolic reactions in the Recon1 metabolic model (*15*) using CORDA (*16*) and cobrapy (*17*) based on the RNA-seq profiled expression levels of the genes associated with each metabolic reaction. While applying CORDA, we assigned high expression confidence score 3 to the top 35% highest expressed genes, medium confidence score 2 to the 35% to 85% highest expressed genes, and low confidence score 1 to 85%-100% highest expressed genes, in order to minimize the standard deviation of flux-levels across samples from each group for all groups. In addition, we manually activated the following essential pathways that are considered to be necessary for the model stability, since these essential pathways may not be properly activated based on RNA-seq data alone: 'Oxidative Phosphorylation', 'Citric Acid Cycle', 'Glycolysis/Gluconeogenesis', 'CoA Biosynthesis', 'CoA Catabolism', 'NAD Metabolism', 'Fatty Acid Metabolism', 'Fatty acid activation', 'Fatty acid elongation', 'Fatty acid oxidation', 'ROS Detoxification', and 'Biomass and maintenance functions'. On each context specific genome scale metabolic model, we applied flux balance analysis (FBA) with each reaction as the objective to optimize the flux of the objective reaction. The LP optimization problems were solved by Gurobi solver (Gurobi Optimization, L. L. C., 2020) whose reference manual can be found in https://www.gurobi.com. All modeling procedures were implemented within a Jupyter notebook 6.1.5 using Python 3.7.7 (*18*). While gene expression levels were applied to the modeling procedure by each RNA-seq sample, all other parameters were maintained identically for all RNA-

seq samples. The modeling procedure reported outcome as the FBA generated optimal flux levels of all available reactions of each context specific metabolic model constructed from each RNA-seq sample and the optimal flux levels were analyzed as variables for comparison between grouped cohorts as discussed in the text. Since it is impossible to presume variance or normality of flux distributions within and between cohort groups, a non-parametric Van der Waerden (VdW) test was applied to compare groupwise flux levels using the R matrixTests package (v. 0.1.9). Some pathways were chosen based on mitochondria-associated connection or Covid19-associated peculiarity and selected reactions with significant p values < 0.05.

Analysis of monocyte RNA-seq data

The monocyte COVID-19 RNA-seq data, published under the accession GSE159678 (*19*), was downloaded from SRA and gene expression was quantified using Salmon's selective alignment approach (*20*). The RNA-seq processing pipeline was implemented using pyrpipe (*21*) (https://github.com/urmi-21/pyrpipe/tree/master/case_studies/Covid_RNA-Seq). Exploratory data analysis and differential expression analysis were performed using MetaOmGraph (*22*).

Analysis combining autopsy and nasopharyngeal swab RNA-seq data

To combine the results from the autopsy and nasopharyngeal swab RNA-seq data, we utilized the t-score values from the DESeq2 analysis. Heatmaps were displayed using pheatmap (*23*). Circular heatmaps were produced in R (version 4.1.0), using the Complex Heatmap (*24*) (version 2.9.4) and circlize (*25*) (version 0.4.12) packages.

Analysis of COVID-19 murine tissue RNA-seq data

From the RNA-seq data the reads were aligned to the *Mus musculus* BALB/c or C57B/6 genome (v1.100) and the SARS-CoV-2 genome MA10 (MT952602) using the CLC Genomics Workbench v20.0 (https://digitalinsights.qiagen.com/) with the RNA-seq and Small RNA Analysis pipeline and the RNA-Seq Analysis module with all standard settings, the read counts then calculated. From the pipeline the fold-change and p-adjusted values were calculated and utilized for all downstream analysis similar to the autopsy data. The murine RNA-seq data has been deposited in the NCBI BioProject database (https://www.ncbi.nlm.nih.gov/bioproject/) under the BioProject accession number PRJNA803057.

Gene Set Enrichment Analysis (GSEA)

For pathway analysis, we utilized fast Gene Set Enrichment Analysis (fGSEA) (*26*). Pathway analysis was done utilizing custom-made Gene Set files from either MitoPathway or the genes we curated available in the **Tables S2&S3**). Using fGSEA, all samples were compared to controls and the ranked list of genes was defined by the t-score statistics. The statistical significance was determined by 1000 permutations of the genesets (*27*).

Proteomic and transcriptomic analysis in the blood tissue and nasopharyngeal samples and CaCo-2 cells.

The nasopharyngeal relative mRNA level change between severe and uninfected subjects. Changes in host protein levels are from published 24 hours post-infection CaCo-2 cells mass spectrometry-based proteomic data (*28*) (https://www.nature.com/articles/s41586-020-2332-7). 2D annotation enrichment for RNA-seq and proteomics data was performed using Perseus 1.6.14.0 for proteomic and transcriptomic analysis of the mitochondrial genes (*29*)

(https://www.nature.com/articles/nmeth.3901 and (*30*) https://bmcbioinformatics.biomedcentral.com/articles/10.1186/1471-2105-13-S16-S12).

   We downloaded whole blood transcriptome data and plasma proteome data from The COVIDome Explorer Researcher Portal (*31*). We used the following filters for transcriptome data: Category "Effect of COVID-19 status", Platform "Blood", Statistical test "Student's t-test", Adjustment method "none", Sex "male" and "female", Age Group "All". We used similar filters for proteome data: Category "Effect of COVID-19 status", Platform "SOMAscan", Statistical test "Student's t-test", Adjustment method "none", Sex "male" and "female", Age Group "All". We analyzed mitochondrial genes at both transcriptome and proteome levels and visualized the data using RStudio Desktop 1.3.1093 (*32*), ggplot2 version 3.3.2 and ggrepel version 0.8.2 ggrepel (*33*).

Gene Symbol	Function	RNA BALF (1) LUNG (2)		Protein CaCo2(1) hPAEpiC(2)	
OXPHOS					
COQ6	Ubiquinone synthesis	[red]	1	[light blue]	1,2
COQ7	Ubiquinone synthesis	[red]	1		
COQ8A/B	Coenzyme Q synthesis			[light blue]	2
Complex I					
TMEM126B	Complex I assembly factors & subunits	[blue]	1		
NUBPL				[light blue]	2
NDUFA1		[blue]	1		
NDUFA4				[light blue]	1,2
NDUFA6		[blue]	1		
NDUFA7				[red]	1
NDUFA11				[red]	2
NDUFA13		[red]	1		
NDUFAB1		[blue]	1		
NDUFAF6		[blue]	1		
NDUFB1		[blue]	2		
NDUFB2					
NDUFB4		[blue]	1		
NDUFB7		[blue]	2		
NDUFB9		[blue]	1		
NDUFC1		[blue]	1		
NDUFS4		[blue]	1		
NDUFV1		[blue]	1		
NDUFA4L2		[blue]	2		
NDUFA4L2		[red]	1		
Complex II					
SDHAF2	Complex II assembly factor	[blue]	**1**	[light blue]	**1**
SDHA	Complex II subunit	[blue]	1		
Complex III					
UQCC1	Complex III assembly			[light blue]	1
UQCC2	Complex III assembly	[blue]	2		
UQCR10	Complex III subunit	[blue]	1		
UQCR11	Complex III subunit	[blue]	1		
UQCRC1	Complex III subunit	[red]	1		
UQCRQ	Complex III subunit	[blue]	1		

Gene Symbol	Function	RNA BALF (1) LUNG (2)		Protein CaCo2(1) hPAEpiC(2)	
OXPHOS					
Complex IV					
SCO2	Complex IV assembly			[light blue]	1
CMC1				[light blue]	2
COA3		[blue]	1	[light blue]	2
COA4		[blue]	**1**	[light blue]	**1,2**
COA5		[blue]	2		
COA6		[blue]	**1**	[light blue]	**1**
COX5A	Complex IV subunit	[blue]	1		
COX6A1		[blue]	1		
COX6B1		[blue]	1		
COX7B		[blue]	1		
COX7C		[blue]	1		
COX16				[light blue]	1
Complex V					
ATP5PF	Complex V subunit			[light blue]	1,3
Metabolism					
Glycolysis					
HK1	Catalyzes glucose to glucose-6-phosphate	[red]	1,2		
HK2		[red]	**1**	[red]	**1**
HK3		[red]	1		
HKDC1	Catalyzes hexose to hexose 6-phosphate.			[red]	1
GPD1	Glycerol-3-phosphate dehydrogenase	[red]	1		
PKM	Pyruvate kinase M1/2	[red]	1		
TCA Cycle					
PDPR	Regulator of pyruvate dehydrogenase	[red]	1		
ME2	Mitochondrial NAD-dependent malic enzyme			[red]	1
ME3		[red]	1		
Mitochondrial Protein Import/Translation					
NOA1	Mitochondrial translation/respiration			[light blue]	2
TIMM8B	Mitochondrial membrane import proteins	[blue]	**1**	[light blue]	**1,2**
TIMM23				[light blue]	1,2
TOMM5		[blue]	2		
TOMM7		[blue]	1		
TOMM40		[red]	1		

Fig. S1. Conserved protein and transcript level changes in SARS-CoV-2 infection cells and tissues. We compared changes in host protein levels from infected CaCo-2 cells extracted from Bojkova *et al.* 2020 (*28*) (Protein 1) and human pulmonary alveolar epithelial cells (HPAEpiC) extracted from Wang *et al.* 2020 (*34*)(Protein 2) with changes in transcript levels from SARS-CoV-2 infected BALF (RNA 1) and lung autopsy (RNA 2) samples extracted from Miller *et al.* 2021(*35*). Blue squares represent decreased protein/RNA levels. Red squares represent increased protein/RNA levels. Bold red font represents conserved changes in both protein and transcript levels.
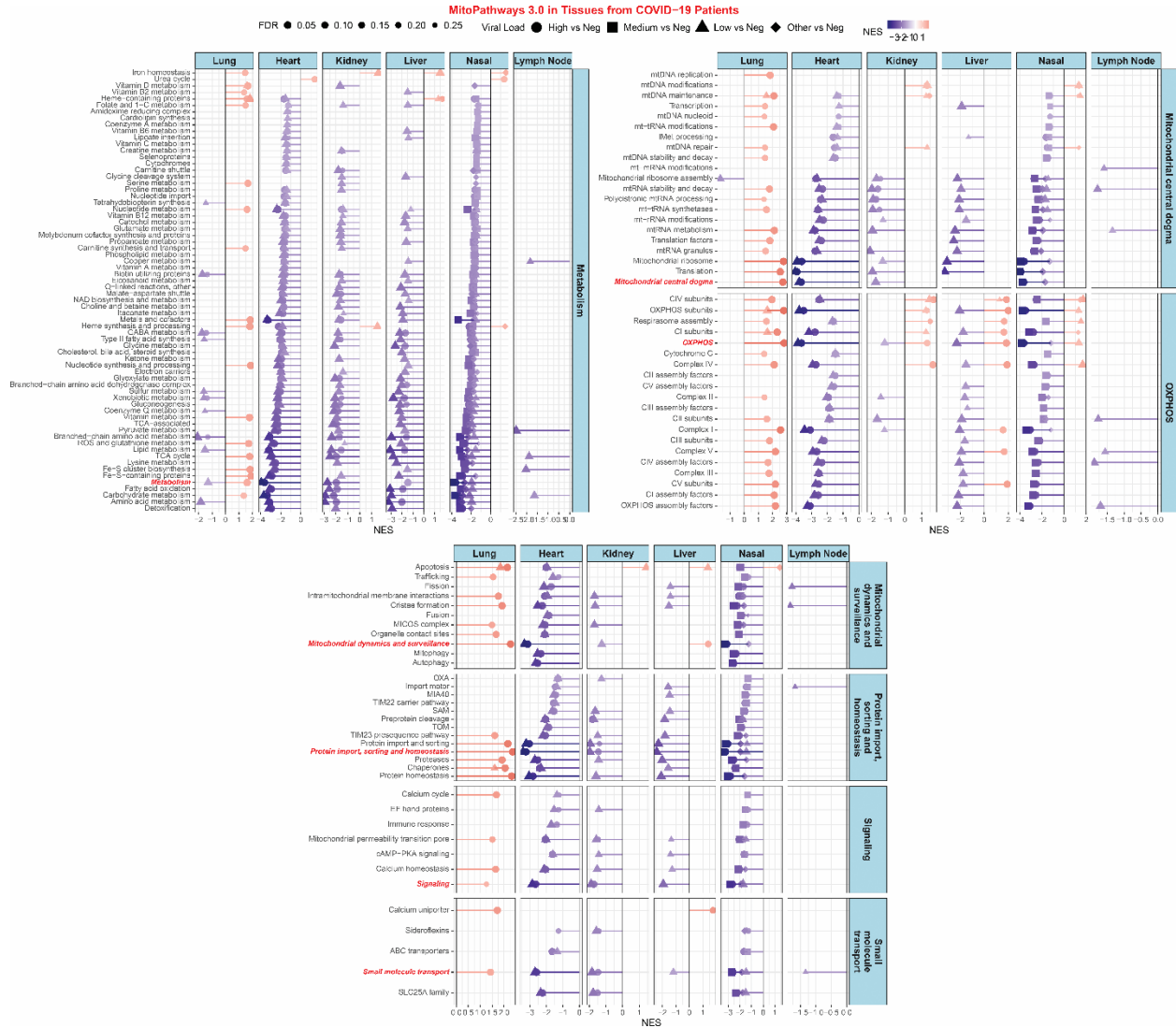
Fig. S2. Lollipop plots for statistically significant MitoPathway gene sets determined by fGSEA. Only pathways with a FDR ≤ 0.25 are displayed. NES = nominal enrichment score.
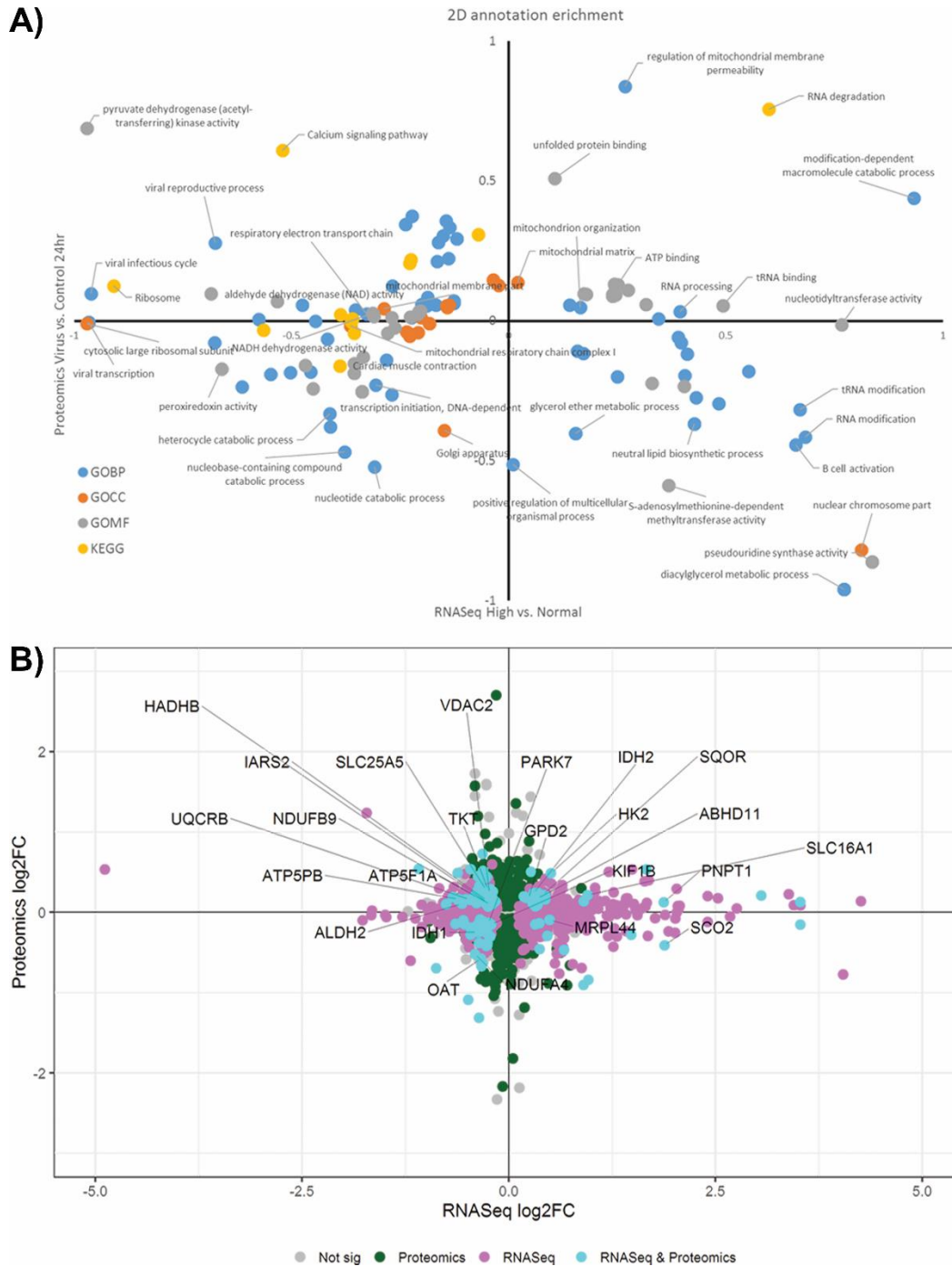
Fig. S3. Correlation between mitochondrial protein and genes determined from MitoCarta.
A) Gene Ontology (GO) analysis determined from nasopharyngeal RNA-seq patient data from high vs negative viral load compared to proteomic data from infected CaCo-2 cells (*28*). **B)** Mitochondrial genes overlapping between nasopharyngeal RNA-seq patient data from high vs negative viral load compared to proteomic data from infected CaCo-2 cells (*28*).
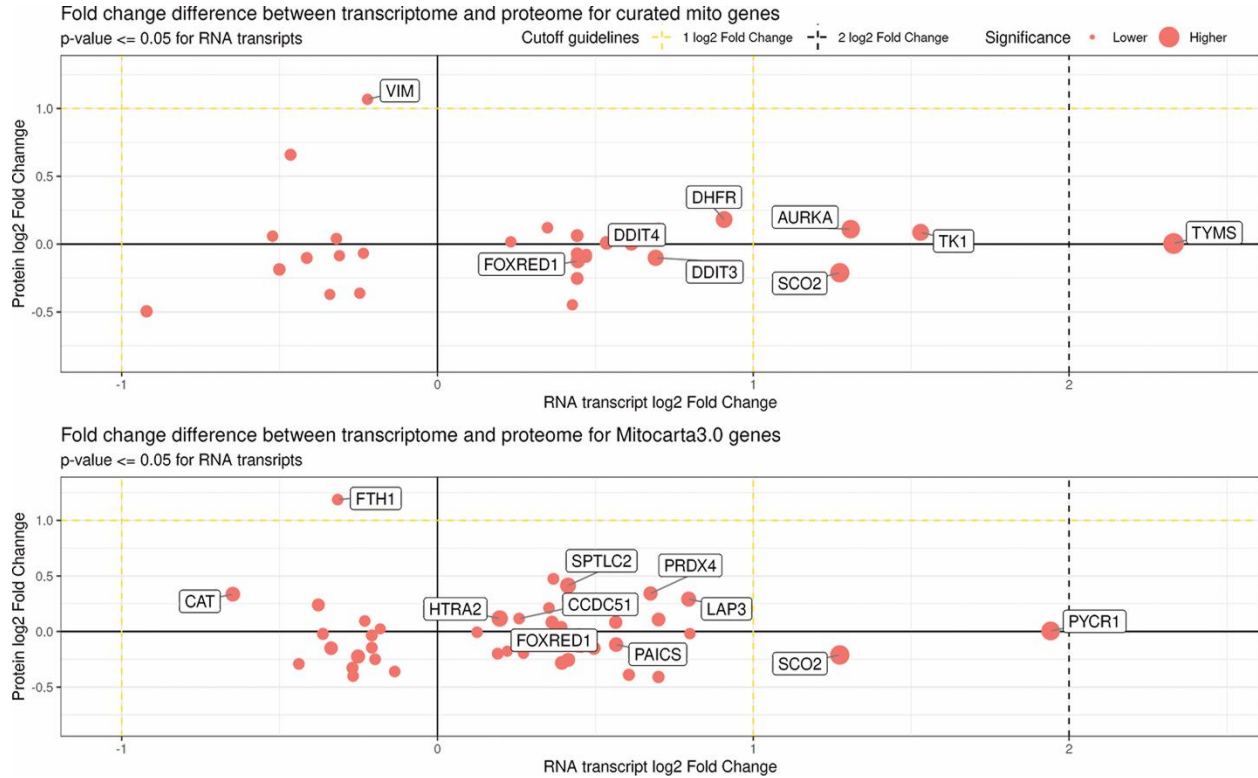
Fig. S4. Correlation between mitochondrial protein and genes determined from MitoCarta in blood from COVID patients. Mitochondrial specific genes determined from our curated mitochondrial genes (top graph) and MitoCarta genes (bottom graph) comparing protein and RNA transcript changes in the blood from COVID patients (determined from COVIDome)(*31, 36*).

Fig. S5. Metabolic flux analysis on RNA-seq data from nasopharyngeal and autopsy patient. **A)** Metabolic fluxes associated with fatty acid biogenesis. **B)** Metabolic fluxes associated with cofactor metabolism. For both **A) and B)** Upset plots are on the overlapping up- and down-regulation metabolic fluxes with the nasopharyngeal and autopsy RNA-seq patient samples. The red color dots represent the up regulated metabolic fluxes and the blue color dots represent the down regulated fluxes. The bar chart on top are the number of overlapping metabolic fluxes for each intersect. The set size bar plot represents the total number of metabolic fluxes contained in each row. Heatmaps of the of the $\log_2$ fold-change values for the significantly regulated fluxes in the major group flux pathways designated by the top or left color bar. The color bar represents the $\log_2$ fold-change values.

Protein	Gene Symbol	Function	Citation
Polypeptides of mitochondrial protein synthesis			
M	TARS2	Mitochondrial leucyl-tRNA synthetase	37,38
	NARS2	Mitochondrial asparaginyl-tRNA synthase	39
Polypeptides of OXPHOS			
Nsp6	ATP5MG	"g" subunit of the mitochondrial ATP synthase	37,38
	ATP5F1E, ATP5F1B, ATP5PB, ATP5PD, ATP5F1D, MT-ATP6	Subunits of the mitochondrial ATP synthase	39
M	**COQ8B**	**Coenzyme Q synthesis protein**	**37-39**
Polypeptides of the mitochondrial cytosolic protein import apparatus			
M	PMPCA	Mitochondrial transit protease	37,38
	PMPCB	**Mitochondrial transit protease**	**37-39**
	PITRM1	**Mitochondrial pre-sequence protease**	**37-39**
Orf9b	**TOMM70**	**Outer mitochondrial membrane import protein**	**37-41**
Orf10	TIMM8B	Inner mitochondrial membrane import protein	37,38

Table S1. Conserved Host-SARS-CoV-2 Mitochondrial Protein Interactions. We performed a comparative analysis of interactions between SARS-CoV-2 polypeptides and host mitochondrial proteins using data generated from three separate studies, Gordon et al. 2020 (*37*), Gordon et al. 2020 (*38*), and Stukalov et al. 2021 (*39*), via MitoCarta alignment. Jiang et al. 2020 (*40*) and Wu et al. 2020 (*41*) are two additional studies that validated the Orf9b-TOMM70 interaction. Bold red font represents Host-SARS-CoV-2 interactions conserved between three or more studies.

Table S2. Curated mitochondrial genes utilized for Figs. 1 - 4.

mtDNA GENE COMPLEMENT
The mtDNA codes for 7 of the 45 proteins of complex I (MT-ND1, MT-ND2, MT-ND3, MT-ND4, MT-ND4L, MT-ND5, MT-ND6), 1 of the 11 subunits of complex III (MT-CYB), 3 of the 13 subunits of complex IV (MT-CO1, MT-CO2, MT-CO3), and 2 of the approximately 17 subunits of complex V (MT-ATP6, MT-ATP8), plus the 22 tDNAs and 12S and 16S rRNAs for the translation of the mtDNA mRNAs. mtDNA genes are highlighted in red below.

MITOCHONDRIAL OXPHOS:
Complex I:
Q-Module:
Structural Subunits: NDUFS2, NDUFS3, NDUFA5, NDUFS7, NDUFS8,
Assembly Factors: NDUFAF3, NDUFAF4, NDUFAF5, NDUFAF6, NDUFAF7.

P$_{p-a}$-Module: [Q/ND1-Module]
Structural Subunits: MT-ND1, NDUFA3, NDUFA9, NDUFA13, NDUFA8.
Assembly Factors: TIMMDC1, NDUFAF2

P$_{p-b}$-Module: [ND2-Module]
Structural Subunits: MT-ND2, MT-ND3, MT-ND6, MT-ND4L, NDUFA1, NDUFA10, NDUFC1, NDUFC2, NDUFS5.
Assembly Factors: NDUFAF1, ECSIT, ACAD9, COA1, TMEM126B, TMEM186

P$_{D-a}$-Module: [ND4-Module]
Structural Subunits: MT-ND4, NDUFB1, NDUFB4, NDUFB5, NDUFB6, NDUFB10, NDUFB11,
Assembly Factors: FOXRED1, ATP5SL, TMEM70

P$_{D-b}$-Module: [ND5-Module]
Structural Subunits: MT-ND5, NDUFAB1, NDUFB2, NDUFB3, NDUFB7, NDUFB8. NDUFB9.
Assembly Factors: DMAC1/TMEM261

N-Module:
Structural Subunits: NDUFVI, NDUFV2, NDUFV3, NDUFA2, NDUFA6, NDUFA7, NDUFA11, NUDFA12, NDUFS1, NDUFS4, NDUFS6.
Assembly Factors: NUBL

Holoenzyme Antioxidant factor: AIFM1

Complex II:
Structural Subunits: SDHA
Assembly Factor: SDHAF2, SDHAF4,
Structural Subunits: SDHB.

14

Assembly Factor: SDHAF1, SDHAF3,
Structural Subunits: SDHC, SDHD

Complex III:
Structural Subunits: MT-CYB, UQCRB, UQCRQ.
Assembly Factors: UQCC1, UQCC2, UQCC3.
Structural Subunits: CYC1, UQCRC1, UQCRC2, UQCRH, UQCR10
Structural Subunits: UQCRFS1
Assembly Factors: MZM1L/LYRM7, BCS1L
Structural Subunits: UQCR11
Assembly Factors: TTC19

Complex IV:
MITRAC Module:
Structural Subunits: MT-COI.
Assembly Subunits: LRPPRC, TACO1, COA3, COX14, CMC1, COX10, COX15, COX11, COX17, COX19, COA1, SURF1, MTRAC7.

MT-CO2-Module:
Structural Subunits: MT-CO2, COX5B, COX6C, COX7B, COX7C, COX8A. Plus??: COX4i1, COX5A
Assembly Factors: COX20, COX18, COX16, COA6, SCO2, SCO1, TMEM17, PET100, PET117, MR-1S.

MT-CO2-Module:
Structural Subunits: MT-CO3, COX6A, COX6B1, COX7A, NDUFA4
Assembly Factors: None known?

Complex V:
F1-Module:
Structural Subunits: ATP5F1A (α), ATP5F1B (β), ATP5F1C (γ), ATP5F1D (δ), ATP5F1E (ε)
Assembly Factors: ATPAF1 (ATP11), ATPAF2 (ATP12), ATP5IF1 (F1)

C8-Ring:
Structural Subunits: ATP5MC1/2/3 (c)
Assembly Factors: ATPSCKMT

Peripheral Arm Subunits:
Structural Subunits: ATP5PB (b), ATP5PD (d), ATP5PF (F$_6$) ATP5PO (OSCP), ATP5ME (e), ATP5MG (g), ATP5MF (f)
Assembly Factors: Unknown

Holoenzyme Completion: MT-ATP6, MT-ATP8, ATP5MJ (6.8), ATP5MK (k, DAPIT)
Structural Subunits: ATP5S(DMAC2L), TMEM70, FMC1

MITOCHODRIAL BIOGENESIS

mtDNA replication: POLG1, POLG2, TFAM.

mtDNA transcription: mtDNA-POLMT, TFB1M, TFB2M nDNA-(PPAR = peroxisome proliferator-activated receptor): PPARα, PPARβ, PPARγ. PGC-1α (PPARGC1A), PGC-1β (PPARGC1B), and PRC (PRC1), NRF1, NRF2, CHCHD2 (MNRR1).

MITOCHONDRIAL METABOLISM
Folate Single Carbon Metabolism:
Mitochondrial:
DHFR2, SHMT2, MTHFD2, GTPBP3/MTO1, ALDH1L2 MTFMT, GCS, GTPBP3/MT01
Nuclear-Cytosol:
DHFR, SHMT1, SHMT2a, MTHFD1, MTHFR, MTR

ATP/NAD$^+$ Carriers:
SLC215A1 (citrate transporter), *SLC25A12* (aspartate/glutamate carrier, Aralar1), *SLC25A3* (phosphate carrier), *SLC25A4* (ANT1), *SLC25A5* (ANT2), SLC25A6 (ANT3), *SLC25A24* and *SLC25A25 (*ATP-Mg/Pi carriers).

Additional Carriers:
NCLX, MCU (genes = MICU1, MICU2, EMRE, MICU1, MICU2, MICU1.1, MCUR1), NHE, LETM1.

CoQ Synthesis:
TAT, AADAT, ALDH3A1, PDSS1, PDSS2, CoQ2, CoQ6, CoQ3, CoQ5, CoQ8a/b, CoQ7, CoQ9, CoQ3

TCA Cycle:
PDHA1, PDHA2, PDHB, PDK1, CS, ACO1, IDH1, IDH2, IDH3A, OGDH, SUCLA2, SUCLG1, SDHA, SDHB, SDHC SDHC1, FA, MDH1, MDH2, GS, GDH (Glutamine to α-ketoglutarate).

Fatty Acid Oxidation:
SLC22A2, SLC22A5, CPT1A, CPT2, HADH, HADHA, HADHB, HADHSC, ACAA2, DECR1, ACADS, ACADM, ACADVL, ETFA, ETFB, ETFDH, DECR1.

Fatty Acid Synthesis (mtFASII):
ACC1, NDUFAB1/ACP, ACSF3, ACACA, AASDHPPT, MCAT, OXSM, HTD2, MECR, CBR4, HSD15B8, HTD2, FADS1,

Urea Cycle:
CPS1, OTC, ASS, ASL, ARG1.

Cytosolic Protein Import:
Translocase outer membrane (TOMM): TOMM20, TOMM22, TOMM5, TOMM7, TOMM40, TOMM6, TOMM70, TOMM71.

16

Translocase Inner Membrane (TIMM): TIMM10, TIMM18, TIMM17, TIMM16, TIMM44, TIMM22, TIMM23, TIMM50, PAM.

Pre-sequence Cleavage: PMPCA, PMPCB, PAM16, ICP55, OCT1, MGE1. Carrier Complex: TIM22, TIM18, TIM54, TIM9, TIM10, TIM12.

Thioprotein Import: MIA40, ERY1, HOT13, CHCHD4,

B Barrel Import Outer Membrane: TOMM35, TOMM36, SAM50.

TOMM40 Import: MDM10, TOMM7, MDM12, MDM34, MMM1, GEM1.

A Import Outer Membrane: MIM2, MIM2.

Mitochondrial Contact Sites: OPA1, MIC 19, MIC60, MIC10, MIC12, MIC27, MIC26.

Mitochondrial Fusion-Fission:
OPA1, MFN1, MFN2, DRP1.

Mitophagy:
PINK1, PARKN, BNIP3, NIX, FUNDC1, FXBP8, Bcl2L13, AMBRA1, LC3, LC3A, LC3B, GABARAP, SIAH-1, ARIH1, MUL1, OPTN, NDP52, PLS3.

ANTIOXIDANT DEFENSES:
SOD1, SOD2, GPX1, GPX4, TXN (thioredoxin), TXN2, TRXR (thioredoxin reductase) PRX (peroxiredoxins), GR (Glutathione reductase), APE1(Ref-1/AP endonuclease), Nrf2, KEAP1.

PEROXISOME:
PEX1, PEX2, PEX3, PEX5, PEX6, PEX7, PEX10, PEX12, PEX13, PEX14, PEX26, PHYH, CAT, AGXT, ACOX1, HAD17B4, GNPAT, ABCD1, AMACR, DHAPAT, AGPS, TRIM37, FADS2 and FADS3.

ENERGY SENSING KINASES AND mTOR ACTIVATOR GENES:
AMPK:
PRKAA2, PRKAB1, PRKAG1.
GSK3B-mTOR activator:
GSK3B + STK11, CAB39, STRADA.
REDD1-mTOR activator:
DDIT4.
AKT:
AKT1, AKT2, AKT3.

mTOR STRUCTURAL GENES:
mTORC1:
TSC1, TSC2, RHEB, RPTOR, AK1S1, MTOR, DEPTOR, MLST8, TEL2, TTI1, CLIP-170, GRB10, LIPIN1, ATG1, EIF4EBP1, RPS6KB1
mTORC2:
MAPKAP1, RICTOR, PRR5, PRR5L,

GLYCOLYSIS:
SLC2A1 (GLUT1), SLC2A4 (GLUT4) (Glucose transporters), HKI-III (hexokinases I,II, III) HKIV (glucokinase), GPI (phosphoglucose isomerase), PFKM or PFKL (phosphofructokinase),

ALDOA (aldolase), GAPDH glyceraldehyde phosphate dehydrogenase, PGK 1 (phophoglycerate kinase), ENO1 (enolase), PKM (pyruvate kinase), LDHA (lactate dehydrogenase pyruvate to lactate), or LDHB (lactate dehydrogenase lactate to pyruvate), (), *SLC16A1* (monocarboxylate transporter 1, MCT1) SLC16A3 (MCT4).

GLUCONEOGENESIS
PC (pyruvate carboxylase), PCK1 (*phosphoenolpyruvate carboxykinase* 1), FBP1 (*fructose 1,6-*bisphosphatase), G6PC1 (*Glucose-6-Phosphatase* catalytic subunit) + (glycolysis genes)

HYPOXIA INDUCIBLE FACTOR PATHWAY:
Hypoxia Inducible Factor family of proteins: HIF1A, HIF1B, HIF2A, HIF3A-1.
HIF regulators: VHL, p300, PHD1, PHD2, PHD3.
Selected HIF target genes: VEGF, EPO, PDGFβ, GPI, PGF, CXCL12, CXCLR4,HMOX1, ID2, IGF2, TERT, OCT4, PGM, TGFα, GADD45A, TGFβ3, IGFBP3, NOS2, NOS3, NOX2, NOXA, GPX3, SOD2, ADM, ANGPT1, ANGPT2, ANP, BRCP, CP, EDN1, FECH, FLK1, FLT1, LEP, SERPINE1, TF, CD73, CTGF, ENG, ITF, MET, NR4A1, REDD1, RORα4, STK15, WT1, SNA1, SNA2, TCF3, VIM, ZEB1, ZEB2, BNIP3/3L, NDRG, PP5, MCL1, NPM, AMF, ANGPTL4, CTSC, L1CAM, LGALS1, LOX, LOXL2, LOXL4, MMP1, MMP2, MMP9, MMP14, PLAUR, STC2, TWIST1.
HIF1α regulated mitochondrial genes: COX4-2 (shifts cytochrome c oxidase from the COX4-1 to COX4-2 regulatory subunit, which increases the efficiency of complex IV), PDK1 (induction of pyruvate dehydrogenase kinase 1, which shunts pyruvate away from the mitochondria), BNIP3 (induction of BNIP3 triggers mitophagy), microRNA-210 (induction of microRNA-210 blocks assembly of Fe/S clusters required for OXPHOS).

FATTY ACID SYNTHESIS:
ACACA, ACSLI, FAS, FAD1, FAD2, FAD3

NADPH SYNTHESIS-PENTOSE PHOSPHATE CYCLE:
G6PD, GNL, PGD, RPIA, RPE, TALDO1, TKT.

GLUTATHIONE METABOLISM:
GLCLC, GLCLM, GS, GR, GPX1, GPX2, GPX3, GST [The *GST* gene family comprises 16 genes in six subfamilies -- alpha (*GSTA*), mu (*GSTM*), omega (*GSTO*), pi (*GSTP*), theta (*GSTT*) and zeta (*GSTZ*)].

NUCLEOTIDE SYNTHESIS:
Mitochondrial: RRM2**,** CMPK2, DGOUK, RRM2R, NME4 (NDPKD), MPV17, TK2.
Nuclear: Pyrimidines: RRM1, CAD, DHODH, UMPS, TYMS, TK1, DCK**.**
Purines: PRPS1, PPAT, GART, PFAS, PAICS, ADSL, ATIC, HPRT, APRT

INTEGRATER STRESS RESPONSE:
Cytosolic: ribosomal protein genes; mitochondrial ribosomal protein genes, eIF2α, eIF2β, HRI (EIF2K1), PERK (EIF2AK3), GCN2 (EIF2AKA), PKR (EIF2AK2), XBP1, ATF4, ATF5, ATF6, FGF21, GDF15, SCAF1, GADD34 (PPP1R15A), CHOP (DDIT3).

18

Additional ATF4 target genes: ATF3, BCL-2, NOXA, PUMA, BIM, REDD1, DDIT4, SESN2, anti-mTOR.

MITOCHONDRIAL REGULATION OF INNATE IMMUNITY:
Inflammasome Genes: NLRP3, ASC, procaspase-1, proIL-18, proIL-1β, IL-R1, MyD88, IKBα, RelA, NFKB. CMPK2.
Interferon Pathway Genes: cGAS, STING, TBK1, IRF3, INFα, INFγ, STAT1, STAT2, IRF9
Notes:

Table S3. Representative Volcano Plot Genes that are Differentially Regulated.

I. **Nasopharyngeal Sample Deferentially Regulated Genes**

A. **Up Regulated Genes**

CMPK2-cytosine monophosphate kinase 2-rate limiting step of mtDNA replication whose induction is central to the creation of Ox-mtDNA which is released from the mitochondrion to activate the inflammasome (*42*).

PNPT1-polyribinucleotide nucleotidyltransferase 1-thought to be involved in processing mitochondrial double stranded RNA released into the cytosol to engage MDA5-driven anti-viral signaling and trigger the Type I interferon response (*43*).

IF!27-interferon Alpha Inducible Protein 27- which in blood is the transcript that provides the greatest discrimination between SARS-CoV-2 positive and negative samples (*36*).

SCO2-Cyrtochrome c oxidase assembly factor.

SLC25A28-Mitoferrin-2-mitochodnrial iron transported for heme and Fe/s synthesis.

PPM1K-Mg/Mn dependent protein phosphatase-regulated branched chain keto-acid dehydrogenase and the permeability transition pore.

BCL2L13-regulates apoptosis.

ACOT9-Acyl-CoA Thioesterase 9-which regulates fatty acid synthesis.

SLC25A3-phosphate carrier-critical for ATP synthesis.

ARS2-RNA-mediated gene silencing, RNAi.

ACOD1-Aconitate decarboxylase 1 or IRG1-which regulates immunometabolism in inflammation and infection (*44*)

B. **Down Regulated Genes**

ATP5PB-ATP Synthase Peripheral Stalk-Membrane Subunit B.

PDK3-Pyruvate Dehydrogenase Kinase 3.

ALDH2-Aldehyde Dehydrogenase 2.

GLS2-L-Glutaminase, liver isoform-which catalyzes the conversion of glutamine to glutamate and ammonia. AASS-Aminoadipate-Semialdehyde Synthase-for lysine degradation.

II. **Autopsy Sample Differentially Regulated Genes**

A. **Heart**

1. **Up regulate Genes**

MUCB-component of the mitochondrial calcium uniporter.

CYP24A1-regulates vitamin D and Ca^{++} and PO_4^{-} levels.

CMPK2, cytosine monophosphate kinase 2-mtDNA replication.

PIF-1-5'-3 'helicase for G-quadruplex resolution-mtDNA replication.

ANGEL2-3'-5'-exoribonucelar and 3' UTP binding protein-mtDNA replication.

CASP8-caspase of caspase 3-cell death & inflammation regulation.

C15orf4-COX protein that on viral infection displaces NDUFA4 to reduce $\Delta\psi$ and mROS plus generates miR-147b that inhibits NDUFA4 mRNA and enhances RIG-1/MDA-5 mediated viral immunity (*45*).

KMO-tryptophan metabolism and cytokine activation.

CA5A-carbonic anhydrase.

CLDC-glycine cleavage.

AGMAT-putrescine synthesis.

2. Down Regulated Genes

GPAM-glycerol-3-phosphate acyltransferase-commitment step of glycerol-lipid synthesis.

SPRYD4-gene of unknown function.

SDHC-complex II subunit.

BCSIL-complex III assembly factor.

COX8A-complex IV structural gene.

HOGA1-lipoic acid synthesis gene.

ACAD8, ACADSB, BDH1-genes involved in fatty acid oxidation.

CKMT1B-creatine-phosphate generation.

PEX11B-peroxisome assembly.

ABCD1-peroxisome enzyme-adrenoleukodystrophygene

ABAT-GABA catabolism

ADHFE1, alcohol dehydrogenase.

AASS, lysine degradation.

ACAT1, acetyl-CoA acetyltransferase.

AFG3L2-AAA peptidase, a spinocerebellar atrophy gene (SCA) gene.

AURKA1P1-aurora-A degradation.

MRM2-rRNA methyl transferase.

QDPR-p53 regulation.

ALAS1-5'-aminoleukinate synthase 1-rate limiting step of protoporphyrin synthesis, heme metabolism.

ABCB7-transport of heme out of mitochondria.

B. Kidney

1. Up Regulated Genes

MCUB-mitochondrial Ca^{++} uniporter related genes-seen in heart.

CCDC90B-mitochondrial protein.

PRIMPOL-primase mtDNA replication.

POLQ-polymerase theta repair gene.

MTERF3-transcription factor.

CASP3-caspase-apoptosis related gene.

BCL2A1, pro-/anti-apoptosis related gene.

RMC10, possible p53 regulator.

NRDC-proteases cleaves at arginines.

ALAS2, 5-aminolevulinate sythetase-heme metabolism gene.

HSCB, iron-sulfur center chaperon.

MTHFD2, methylenetetrahydrofolate dehydrogenase), single carbon metabolism.

ACSM4-fatty acid oxidation.

PRELIOD2, LYPLAL1-lipid metabolism.

OTC-ornithine transcarbamylase-urea cycle.

CYP11B-cytochrome 450 converts progesterone to cortisol-sterol metabolism.

AKAP10-mitochondrial anchor protein for protein kinase A.

MT-ND6, MT-CO1, MT-ATP6-mtDNA transcripts.

2. Down Regulated Genes

GLDC-glycine cleavage-up regulated in the autopsy heart.

SDHA-subunit of complex II-SDHC is down regulated in the heart.

ADCK1-regulates coenzyme Q biosynthesis.

ACACB-generates malonyl-CoA to initiation of mitochondrial fatty acid synthesis (mtFASII) by malonyl CoA-acyl carrier protein transacylase.

ACAD8, ACAD10, ACOT11, ARF5-fatty acid oxidation genes.

ACSS1-acetyl-CoA synthetase.

ABHD11-stabilizes lipoic acid in α-ketoglutarate dehydrogenase (*46*).

PCK2-phosphoenolpyruvate carboxykinase 2, OAA to PEP.

ABCB8-Fe transport across the inner membrane.

PDF-peptide deformylase-removes the formyl group from the formyl-methionine in mitochondrial peptides.

GATB-converts the miss addition of glutamate on tRNA^{Gln} to glutamine.

COMTD1-methylation.

C. Liver
1. Down Regulated Genes

BNIP3L-pro-apoptotic gene.

ALAS2-5'-aminoleukinate synthase 2-rate limiting step of protoporphyrin synthesis, heme metabolism.

C20rf69-OXPHOS complex regulator.

HIGD1A-COX subunit associated with inflammation.

MT-CO3, MT-ATP6, and *MT-ND6*-mtDNA transcripts.

2. Up Regulated Genes

FASN cytosolic fatty acid synthesis.

 oxidation (ACAD10);

ACACA-acetyl-CoA to malonyl-CoA-mitochondrial fatty acid synthesis ();

BCKDHA-branched α-keto acid metabolism.

MTFP1-mitochondrial fission protein.

D. Lymph Node

ATAD3A mtDNA nucleoid gene.

RECQL4-DNA helicase.

ACSM4-fatty acid oxidation gene.

LDHAL6B-actate dehydrogenase homolog.

SERHL2-potential serine hydroxylase.

1. Down Regulated Genes

MCUB-Ca^{++} uniporter-opposite of heart and kidney.

SIRT4-regulates glutamine metabolism.

ACSL6-fatty acid oxidation gene.

E. Lung
1. Up Regulated Genes

C2orf69; COA6-COX assembly genes.

MTHFD1L, MTHFD2-single carbon metabolism genes.

22

ALAS2-5'-aminoleukinate synthase 2-rate limiting step of protoporphyrin synthesis, heme metabolism

CISD1-iron-sulfur center gene.

HSPD1-heat shock protein gene.

apoptosis factors (BCL2A1),

LAP3-peptidases.

POLQ-DNA repairz.

ACADV1, ACOT9-fatty acid metabolism genes.

2. **Down Regulated Genes**

FASN fatty acid synthetase.

ACADL-fatty acid oxidation gene.

PXMP4, AMACR-peroxisomal enzyme genes.

ALDH2alcohol dehydrogenase.

AKAP1-protein kinase A anchor protein gene.

III. Hamster Differentially Regulated Genes

A. Heart

1. Up regulated genes

Kmo-Kynurenine 3-monooxygenase-L-tryptophan metabolism.

Tmem143-membrane protein-possible tumor suppressor.

Slc25a44-transports branched-chain amino acids [valine, leucine and isoleucine] into mitochondria.

2. Down regulated genes

B. Kidney

1. Up regulated genes

Ndufs7-complex I subunit.

Miga2-regulator of mitochondrial fusion.

Phlcd-polycystic kidney and hepatic disease.

2. Down regulated genes

Ndufa4-complex I subunit.

Glyat-glycine-N-acyltransferase.

C. Lung

1. Up regulated genes

Tsfm-mitochondrial translation elongation factor.

Sod2-Mn superoxide dismutase.

2. Down regulated genes

Mpv171-protects mitochondrial from oxidative stress.

D. Olfactory Bulb

1. Up regulated genes

Mcu-mitochondrial Ca^{++} uniporter.

Tdrkh-enables RNA binding.

2. Down regulated genes

23

Atp5p-mitochondrial ATP synthase subunit 5.
sphk2-sphingosine kinase 2.
LonP1-Lon protease.
Tomm40-protein import apparatus.
Slc25a42-coenzyme A transporter.
Aars2-mitochondrial alanyl-tRNA Synthetase.
Bbc3-BCL2 binding component 3-apoptosis.
CoQ8b-coenzyme Q synthesis.
Slc25a1-citrate carrier.

E. Cerebellum
1. Up regulated genes
Mpv171-protects mitochondrial from oxidative stress.
2. Down regulated genes
Ngrn-Neugrin-Neurite Outgrowth.
Qdbr-quinoid dihydropteridine reductase-tetrahydrobiopterin-BH4 recycling'
Adhfe1-hydroxyacid-oxoacid transhydrogenase.
Slc25a1-citrate carrier.

F. Striatum
1. Up regulated genes
Cox7a2-complex IV subunit.
Ndufa9-complex I subunit.
Ndufb6-complex I subunit.
Fh1-Fumarate hydratase 1.
MT-ND3-mtDNA complex I subunit.
Msrb2-Methionine Sulfoxide Reductase B2.
Otc-ornithine transcarbamylase.
2. Down regulated genes
Fxn5-Friedreich's ataxia gene.
Slc25a44-transports branched-chain amino acids [valine, leucine and isoleucine] into mitochondria.
Alap1-A-Kinase Anchoring Protein 1.
Shmt2-mitochondrial serine hydroxymethyltransferase 2.
Slc125a1-citrate carrier.
Pycr2-pyrroline-5-carboxylate reductase 2.
Co8b-coenzyme Q synthesis.
Ldhd-lactate dehydrogenase D.

IV. Mouse Differentially Regulated Genes
A. C57BL/6
1. Up regulated genes
Gatm-glycine amidinotransferase.
Acod1-aconitate decarboxylase 1-inhibition of inflammatory response..
Cmpk2-cytidine/uridine monophosphate kinase 2-mtDNA replication.

Casp8-caspase 8.

Prdx4-peroxiredoxin 4.

Mthfd2-methylenetetrahydrofolate dehydrogenase-NADP+ dependent 2.

Bid-proapoptotic.

Fth1-ferritin heavy chain 1.

Bak1-proapoptotic.

Aldh18a-aldehyde dehydrogenase 18 Family Member A1.

Ak2-adenylate kinase 2,

Kars-lysyl-tRNA synthetase.

Abcd2-transport of very long chain fatty acid-CoA from the cytosol to the peroxisome.

2. Down regulated genes

Alas2-5'-aminolevulinate synthetase, heme synthesis.

Acac-acetyl-CoA carboxylase, biotin containing enzyme.

Aldh6a-aldehyde dehydrogenase.

Cat-catalase.

Bcl2l11-pro-apoptotic gene.

Aass-aminoadipate-semialdehyde synthase.

Abat-4-aminobutyrate aminotransferase.

B. Balb/c

1. Up regulated genes

Cmpk2-cytidine monophosphate kinase 2-mtDNA replication.

Gatm-glycine amidinotransferase.

Fih1-ferritin heavy chain 1.

Acod1-aconitate decarboxylase 1-inhibition of inflammatory response.

Abhd11-lipoylation of the 2-oxoglutarate dehydrogenase complex.

Aurkaip1-aurora kinase A interacting protein 1.

Mrpl51-mitochondrial ribosomal protein L51.

Cisd3-mitochondrial CDGSH iron-sulfur domain-containing protein 3.

2. Down regulated Genes

Alas2-5'-aminolevulinate synthetase, heme synthesis.

Abat-4-aminobutyrate aminotransferase.

Ascl1-Achaete-Scute Family BHLH Transcription Factor 1.

Aass-aminoadipate-semialdehyde synhase.

Fam162a-transformation-dependent protein, HGTD-P.

References

1. D. Butler *et al.*, Shotgun transcriptome, spatial omics, and isothermal profiling of SARS-CoV-2 infection reveals unique host responses, viral diversification, and drug interactions. *Nat. Commun.* **12**, 1660 (2021).

2. J. Park *et al.*, System-wide transcriptome damage and tissue identity loss in COVID-19 patients. *Cell Rep Med* **3** 100522, ePub ahead of print, https://www.cell.com/cell-reports-medicine/fulltext/S102666-103791(100522)100022-100522 (2022).

3. S. Leist *et al.*, A mouse-adapted SARS-CoV-2 induces acute lung injury and mortality in standard laboratory mice. *Cell* **183**, 1070-1085.e1012 (2020).

4. S. Durinck *et al.*, BioMart and Bioconductor: a powerful link between biological databases and microarray data analysis. *Bioinformatics* **21**, 3439-3440 (2005).

5. S. Durinck, P. T. Spellman, E. Birney, W. Huber, Mapping identifiers for the integration of genomic datasets with the R/Bioconductor package biomaRt. *Nat Protoc* **4**, 1184-1191 (2009).

6. D. M. Emms, S. Kelly, OrthoFinder: phylogenetic orthology inference for comparative genomics. *Genome Biology* **20**, 238 (2019).

7. M. D. Robinson, D. J. McCarthy, G. K. Smyth, edgeR: a Bioconductor package for differential expression analysis of digital gene expression data. *Bioinformatics* **26**, 139-140 (2010).

8. M. I. Love, W. Huber, S. Anders, Moderated estimation of fold change and dispersion for RNA-seq data with DESeq2. *Genome Biol.* **15**, 550 (2014).

9. P. A. Ewels *et al.*, The nf-core framework for community-curated bioinformatics pipelines. *Nat. Biotechnol.* **38**, 276-278 (2020).

10. A. Dobin *et al.*, STAR: ultrafast universal RNA-seq aligner. *Bioinformatics* **29**, 15-21 (2013).

11. R. Patro, G. Duggal, M. I. Love, R. A. Irizarry, C. Kingsford, Salmon provides fast and bias-aware quantification of transcript expression. *Nat. Methods* **14**, 417-419 (2017).

12. S. Kovaka *et al.*, Transcriptome assembly from long-read RNA-seq alignments with StringTie2. *Genome Biol.* **20**, 278 (2019).

13. W. A. da Silveira *et al.*, Comprehensive multi-omics analysis reveals mitochondrial stress as a central biological hub for spaceflight impact. *Cell* **183**, 1185-1201 e1120 (2020).

14.   Y. Zhang, M. S. Kim, E. Nguyen, D. M. Taylor, Modeling metabolic variation with single-cell expression data. *bioRxiv* **preprint available at** **https://doi.org/10.1101/2020.01.28.923680** (2020).

15.   N. C. Duarte *et al.*, Global reconstruction of the human metabolic network based on genomic and bibliomic data. *Proceedings of the National Academy of Sciences* **104**, 1777-1782 (2007).

16.   A. Schultz, A. A. Qutub, Reconstruction of tissue-specific metabolic networks using CORDA. *PLoS Comput. Biol.* **12**, e1004808 (2016).

17.   A. Ebrahim, J. A. Lerman, B. O. Palsson, D. R. Hyduke, COBRApy: COnstraints-Based Reconstruction and Analysis for Python. *BMC Syst. Biol.* **7**, 74 (2013).

18.   T. Kluyver *et al.*, in *Positioning and Power in Academic Publishing: Players, Agents and Agendas,* F. Loizides, B. Schmidt, Eds. (IOS Press, 2016), pp. 87-90; DOI: 10.3233/3978-3231-61499-61649-61491-61487.

19.   N. Rother *et al.*, Hydroxychloroquine inhibits the trained innate immune response to interferons. *Cell Rep. Med.* **1**, 100146 (2020).

20.   A. Srivastava *et al.*, Alignment and mapping methodology influence transcript abundance estimation. *Genome Biol.* **21**, 239 (2020).

21.   U. Singh, J. Li, A. Seetharam, E. S. Wurtele, pyrpipe: a Python package for RNA-Seq workflows. *NAR Genom. Bioinform.* **3**, lqab049 (2021).

22.   U. Singh, M. Hur, K. Dorman, E. S. Wurtele, MetaOmGraph: a workbench for interactive exploratory data analysis of large expression datasets. *Nucleic Acids Res.* **48**, e23 (2020).

23.   R. Kolde. (2015).

24.   Z. Gu, R. Eils, M. Schlesner, Complex heatmaps reveal patterns and correlations in multidimensional genomic data. *Bioinformatics* **32**, 2847-2849 (2016).

25.   Z. Gu, L. Gu, R. Eils, M. Schlesner, B. Brors, circlize Implements and enhances circular visualization in R. *Bioinformatics* **30**, 2811-2812 (2014).

26.   G. Korotkevich *et al.*, Fast gene set enrichment analysis. *bioRxiv*, 060012 (2021).

27.   A. Subramanian *et al.*, Gene set enrichment analysis: a knowledge-based approach for interpreting genome-wide expression profiles. *Proc. Natl. Acad. Sci. USA* **102**, 15545-15550 (2005).

28.   D. Bojkova *et al.*, Proteomics of SARS-CoV-2-infected host cells reveals therapy targets. *Nature* **583**, 469-472 (2020).

29. S. Tyanova *et al.*, The Perseus computational platform for comprehensive analysis of (prote)omics data. *Nat Methods* **13**, 731-740 (2016).

30. J. Cox, M. Mann, 1D and 2D annotation enrichment: a statistical method integrating quantitative proteomics with complementary high-throughput data. *BMC Bioinformatics* **13 Suppl 16**, S12 (2012).

31. K. D. Sullivan *et al.*, The COVIDome Explorer researcher portal. *Cell Rep* **36**, 109527 (2021).

32. RStudio Team. (Public Benefit Corporation, Boston, 2020).

33. H. Wickham. (Springer-Verlag, New York, 2016).

34. P. Wang *et al.*, A cross-talk between epithelium and endothelium mediates human alveolar-capillary injury during SARS-CoV-2 infection. *Cell Death Dis.* **11**, 1042 (2020).

35. B. Miller *et al.*, Host mitochondrial transcriptome response to SARS-CoV-2 in multiple cell models and clinical samples. *Sci. Rep.* **11**, 3 (2021).

36. R. K. Gupta *et al.*, Blood transcriptional biomarkers of acute viral infection for detection of pre-symptomatic SARS-CoV-2 infection: a nested, case-control diagnostic accuracy study. *The Lancet Microbe* **2**, e508-e517 (2021).

37. D. Gordon *et al.*, Comparative host-coronavirus protein interaction networks reveal pan-viral disease mechanisms. *Science* **370**, (2020).

38. D. E. Gordon *et al.*, A SARS-CoV-2 protein interaction map reveals targets for drug repurposing. *Nature* **583**, 459–468 (2020).

39. A. Stukalov *et al.*, Multilevel proteomics reveals host perturbations by SARS-CoV-2 and SARS-CoV. *Nature* **594**, 246-252 (2021).

40. H. W. Jiang *et al.*, SARS-CoV-2 proteome microarray for global profiling of COVID-19 specific IgG and IgM responses. *Nat. Commun.* **11**, 3581 (2020).

41. J. Wu *et al.*, SARS-CoV-2 ORF9b inhibits RIG-I-MAVS antiviral signaling by interrupting K63-linked ubiquitination of NEMO. *Cell Rep* **34**, 108761 (2021).

42. Z. Zhong *et al.*, New mitochondrial DNA synthesis enables NLRP3 inflammasome activation. *Nature* **560**, 198-203 (2018).

43. A. Dhir *et al.*, Mitochondrial double-stranded RNA triggers antiviral signalling in humans. *Nature* **560**, 238-242 (2018).

44. R. Wu, F. Chen, N. Wang, D. Tang, R. Kang, ACOD1 in immunometabolism and disease. *Cell Mol Immunol* **17**, 822-833 (2020).

45.   C. Q. E. Lee *et al.*, Coding and non-coding roles of MOCCI (C15ORF48) coordinate to regulate host inflammation and immunity. *Nat. Commun.* **12**, 2130 (2021).

46.   P. S. J. Bailey *et al.*, ABHD11 maintains 2-oxoglutarate metabolism by preserving functional lipoylation of the 2-oxoglutarate dehydrogenase complex. *Nat. Commun.* **11**, 4046 (2020).